Available online at www.sciencedirect.com
SCIENCE DIRECT
Engineering Structures 28 (2006) 869–879
ENGINEERING STRUCTURES
www.elsevier.com/locate/engstruct

A direct displacement-based method for the seismic design of bridges on bi-linear isolation devices

Manuel Jara[a], Joan R. Casas[b,*]

[a] *Civil Engineering School, University of Michoacán, Mexico*
[b] *Civil Engineering School, Technical University of Catalunya, Barcelona, Spain*

Received 1 June 2005; received in revised form 25 October 2005; accepted 25 October 2005
Available online 9 December 2005

Abstract

This paper presents an extension of the displacement-based design procedure for bridges supported on hysteretic isolation bearings. An equivalent damping ratio, derived from the particular characteristics of bridges supported on lead rubber bearings (LRBs), is proposed. The trend of the equivalent damping ratio that is obtained is similar to that of the hysteretic energy bearing dissipation, over the whole range of inelastic displacement demands that is expected for this type of device. The proposed method emphasizes material strain control by means of the lateral displacement of isolator bearings and the lateral displacement of the pier top. The response is obtained directly from the elastic displacement response spectrum and is applicable to regular bridges with rigid superstructures that can be idealized as a single degree of freedom (SDOF) system. The proposed methodology improves the displacement prediction capability of the linear equivalent model when it is applied to bridges supported on LRB isolators, and low data scatter is obtained, especially for displacements. Pier displacements are slightly underestimated and base shears are overestimated, compared to inelastic time-history results.

Keywords: Displacement based design; Equivalent damping ratio; Effective stiffness; Hysteretic isolators

1. Introduction

Recent earthquakes have demonstrated that designing a bridge according to current codes, for a life safety performance, does not assure acceptable structural behavior, even during moderate ground motion [1]. Today it is widely recognized that seismic design codes need to incorporate a performance-based design criterion [2,3], the main objective of which is to ensure that the engineered facilities show satisfactory performance under moderate and extreme earthquake ground motion, according to owners, users and society expectations. A major challenge is the development of rational and effective procedures for analysing and designing structural systems that are capable of predicting the structural response for the earthquake ground motions that are expected to occur during the system life-cycle. Several simplified methods have been proposed for performance-based design: (a) strength-based design, (b) displacement-based design, and (c) energy-based design. A discussion about the characteristics and capabilities of each method can be found in [2,3].

A very simple but reliable conceptual framework called direct displacement-based design has been proposed for achieving the performance-based design objective [3,4]. It is recognized that damage is well correlated to maximum material strain or plastic hinge rotation at the base of piers, which are parameters that can be associated with lateral pier top displacement [3,4]. Based on this, the procedure is focused on displacement, instead of force, as a performance or damage indicator. Although the displacement quantifier is not able to capture the loading path and accumulates over time, as the energy quantifier does, it is receiving a lot of attention because it is simple, effective and allows designers to evaluate the structural performance for various earthquake intensities. Thus, analysis methods for predicting displacement demands are needed.

Typical earthquake protection systems for bridges are seismic isolators in association with passive energy dissipators,

* Corresponding address: Jordi Girona 1-3, Edificio C-1, Ingenieros de Caminos, Canales y Puertos, Campus Norte, Barcelona 08034, Spain. Tel.: +34 93 401 65 13; fax: +34 93 405 41 35.
E-mail address: joan.ramon.casas@upc.edu (J.R. Casas).

0141-0296/$ - see front matter © 2005 Elsevier Ltd. All rights reserved.
doi:10.1016/j.engstruct.2005.10.016

i.e. elastomeric or sliding bearings with dampers or damping mechanisms. Lead rubber bearings (LRBs) are the most commonly used isolators [1], as they provide an economic, reliable and simple solution for protecting medium and short span bridges. This paper presents an extension of the displacement-based design procedure for bridges simply supported on hysteretic isolation bearings. The methodology is applicable to bridges on LRBs, but it can be modified easily for other types of displacement-dependent devices. An extension of the procedure for continuous bridges is also under preparation.

2. Equivalent linearization method

The response spectrum provides some of the most important characteristics of earthquake motion and gives the maximum elastic deformation for structures over the entire range of periods. However, it is not able to predict damage level, as damage involves inelastic deformations. Of course, maximum displacement demands can be obtained through time-history analysis, but in most practical cases linear response spectra or uniform hazard elastic response spectra are used. Hence, many approximate methods have been proposed to overcome this difficulty. Some of them are based on equivalent linearization of the system by using an effective lateral stiffness and equivalent damping ratio. Equivalent linear models have been incorporated in AASHTO [5], Eurocode 8 [6] and Japan Road Association [7], among other specifications, for designing bridges with passive energy dissipation systems.

If it is assumed that the behavior of an inelastic hysteretic structure subjected to ground acceleration $\ddot{x}_g$ can be described by a single degree of freedom (SDOF) system, then the maximum inelastic response is given as,

$$\ddot{x} + 2\xi_i\omega_i\dot{x} + \frac{f_s(x)}{m} = -\ddot{x}_g \tag{1}$$

where x is the mass displacement relative to the ground, ξ_i is the damping ratio, ω_i is the initial circular frequency, $f_s(x)$ is the restoring force, and m is the mass of the system. In the equivalent linearization method, the maximum inelastic displacement demand (x_{eq}) is approximated by,

$$\ddot{x}_{eq} + 2\xi_{eq}\omega_{ef}\dot{x}_{eq} + \omega_{ef}^2 x_{eq} = -\ddot{x}_g \tag{2}$$

where ξ_{eq} is the equivalent viscous damping ratio and ω_{ef} is the effective circular frequency. The appropriate values of ξ_{eq} and ω_{ef} depend on the material hysteretic behaviour, the maximum displacement demand and the number of incursions into the inelastic range, among others. The main difference between the existing equivalent linear methods is the way in which ξ_{eq} and ω_{ef} are determined. The expressions that have been proposed for computing these parameters are based on analytical formulations, empirical relations and/or expressions derived from experimental tests.

As the existing equations for computing ξ_{eq} and k_{ef} may produce inaccurate displacement predictions [8,9], an improved expression for bridges supported on LRB isolators is proposed in this paper. A full description of the most common existing methods for defining ξ_{eq} and k_{ef} (secant stiffness, equivalent damping from one cycle of periodic excitation, Iwan's model [10,11], Kowalsky's model [4]) and some comments about their effectiveness in the prediction of inelastic displacements demands can be found in [12]. In summary, we can say that ξ_{eq}, derived from the harmonic response at maximum displacement, is not capable of incorporating the influence of time-history displacements in the energy dissipation mechanism. During an earthquake, displacements are significantly lower than the maximum response most of the time, and the energy dissipation can be overestimated. The stiffness variation during cyclic deformations cannot be reproduced by the secant stiffness method. As a consequence, local variations in the inelastic spectra cannot be reproduced either. Iwan's formula, derived from numerical minimization of the difference between elastic and inelastic responses, provides the best approximation to these local variations in spectra. Iwan's model is limited to mid-period range structures and $\mu \leq 8$. μ is the ductility factor $= x_{\max}/x_y$, $x_{\max}$ is the maximum displacement of the oscillator and x_y is the yielding displacement. These conditions are different to the expected hysteresis of LRB bearings for bridge isolation. Kowalsky's equation is derived from the Takeda degrading hysteresis model for concrete piers, and is not applicable to LRB isolators either.

According to Ref. [8,9] good approximation can be obtained on average with existing linearization parameters, although there is considerable scatter in the data. Iwan and Gates [13] compared the accuracy of nine damping models for estimating the response of hysteretic bi-linear systems and found that ξ_{eq} is overestimated in all the models for most of the ductility range considered. The frequency content, effective duration, maximum energy input and near fault characteristics of ground motion have not been adequately analysed.

3. An improved ξ_{eq} for bi-linear isolators

The energy dissipation capacity of bearing isolators plays a fundamental role in the effectiveness of damage reduction in bridges subjected to earthquake ground motion. If the equivalent damping ratio is not capable of representing the non-linear energy dissipated by the hysteretic behavior of bearings, then the maximum displacement would not be predicted accurately. Because of the aforementioned weakness of the existing equations, an improved empirical expression is derived in this paper, for the case of bridges supported on LRB bearings.

From the comparison of the overall shape of a family of inelastic response spectra for a given value of μ, with some linear response spectra, it has been found [13] that the difference is very close to a translation along a line of constant spectral displacement, i.e. the linear spectrum for a specific damping coefficient may be translated to fit very closely to the inelastic spectrum for some ductility value. This conclusion is used in this paper to propose the equivalent damping ratio of LRB bearings, as described below.

Assuming k_{ef} as the secant stiffness at maximum displacement, ξ_{eq} is obtained by equating the non-linear displacement response spectrum for a given earthquake to the

Table 1
Characteristics of earthquake ground motion

Earthquake	Station	Duration (s)	PGA (m/s^2)	f (Hz)	PSA (m/s^2)
Imperial Valley, 1940	El Centro	40.00	3.1	2.2	8.3
México 1985	Caleta de Campos	97.24	1.4	1.4	3.9
México 1985	Papanoa	118.10	1.2	4.0	4.7
México 1985	La Unión	124.60	1.5	2.2	5.7
México 1985	SCT	183.51	1.6	0.5	9.4
México 1989	SCT	80.00	0.4	0.5	1.3
Loma Prieta 1989	Corralitos	39.95	6.3	3.3	21.3
Northridge 1994	Santa Barbara	40.00	0.8	3.5	2.6

PGA = peak ground acceleration; PSA = pseudo spectral acceleration.

Table 2
Statistical data for all systems and earthquakes

μ_b	1	2	4	6	8	10	13	18	24	30
$\bar{\xi}_{eq}(\mu_b)$	5.00	6.42	9.72	12.26	16.67	17.66	20.49	21.96	23.55	23.41
$\sigma(\mu_b)$	0.00	1.07	2.56	3.50	3.50	4.59	4.41	3.79	4.95	4.16
CV	0.00	0.17	0.26	0.29	0.21	0.26	0.22	0.17	0.21	0.18
$\bar{\xi}_{eq}(\mu_b) - \sigma(\mu_b)$	5.00	5.35	7.16	8.76	13.18	13.07	16.07	18.17	18.60	19.24

linear displacement response spectrum,

$$S_d(\xi_h, T, \alpha, \mu_b, EGM)_{NL} = S_d(\xi_{eq}, T_{ef}, EGM)_{EL} \tag{3}$$

where $S_d(\xi_h, T, \alpha, \mu_b, EGM)_{NL}$ is the non-linear spectral displacement of a system with hysteretic damping ξ_h, period T, post-yield stiffness ratio α, and bearing ductility μ_b, when it is subjected to a particular earthquake ground motion (EGM), and $S_d(\xi_{eq}, T_{ef}, EGM)_{EL}$ is the spectral displacement of a linear system with viscous damping ratio ξ_{eq} and period T_{ef}, when it is subjected to the same earthquake ground motion EGM. An ensemble of 8 earthquakes, whose characteristics are shown in Table 1, were applied. The acceleration values were scaled in order to obtain different displacement ductility ratios of the isolators.

The LRB bearing properties used for the numerical evaluation are based on code design specifications for bearing isolators [6]. The plan area of the bearings, A_r, satisfies the allowable compression stress for service conditions. The bearing height and lead core diameter meet the design and geometric code recommendations. The initial stiffness is sufficiently high to prevent excessive displacements caused by strong winds, traffic loads or moderate earthquakes. A combination of the LRB properties ($0.05 \le \alpha \le 0.15, 0.05W_s \le F_y \le 0.20W_s, 0.05A_r \le A_l \le 0.10A_r$) are employed in the analysis, where W_s refers to superstructure weight, A_l is the lead core area, and F_y is the shear yield force.

Expected ductility factors of the LRB isolators depend on the limit states defined at the beginning of the design process. Based on experimental data and field-test results, $1 \le \mu_b \le 40$ is considered to be appropriate for the analysis. The bearing ductility is computed as the ratio of the maximum displacement ($x_{\max}$) and the yield displacement of the bearing ($x_y = F_y/k_1$), where,

$$F_y = A_l \tau_y \tag{4}$$

$$k_1 = \frac{1}{\alpha}\frac{G_r A_r}{h_r}\left(1 + 10\frac{A_l}{A_r}\right) \tag{5}$$

in which G_r is the shear modulus, h_r is the total thickness of elastomer, and μ_b is given by,

$$\mu_b = \frac{x_{\max}}{x_y} = \frac{G_r A_r}{\alpha A_l \tau_y h_r}\left(1 + 10\frac{A_l}{A_r}\right) x_{\max} \tag{6}$$

ξ_{eq} is obtained as the viscous damping ratio of the linear system that equalizes both spectra (non-linear and linear) for the combination of all parameters described above. After ξ_{eq} has been obtained for n systems, their sample mean ($\bar{\xi}_{eq}(\mu_b)$) and sample standard deviation ($\sigma(\mu_b)$) is computed for each bearing ductility factor,

$$\bar{\xi}_{eq}(\mu_b) = \frac{1}{n}\sum_{i=1}^{n} \xi_{eq_i}(\mu_b) \tag{7}$$

$$\sigma(\mu_b) = \sqrt{\frac{1}{n-1}\sum_{i=1}^{n}\left[\xi_{eq_i}(\mu_b) - \bar{\xi}_{eq}(\mu_b)\right]^2}. \tag{8}$$

The histograms of ξ_{eq} for μ_b values equal to 2, 4, 6, 8, 10, 13, 18, 24, 30 were computed, where all variables (earthquakes, post-yield stiffness values and initial system stiffness) were taken together [12]. In general, the ξ_{eq} distribution for all ductility levels resembles the normal distribution. Assuming a normal probability distribution, the probabilities of exceeding 50% and 84.1% represent the mean value and mean value minus one standard deviation, respectively. These data are given in Table 2, where it can also be seen that the scattering of data increases for higher inelastic displacement demands, with a maximum $\sigma(\mu_a) = 4.95$ for $\mu_b = 24$. However, the coefficient of variation (the ratio between standard deviation and the mean) increases with the ductility factor, up to a maximum of 0.285 for $\mu_b = 6$, and is rather uniform for higher ductility displacements (Fig. 1). Unfortunately, maximum dispersion occurs in the

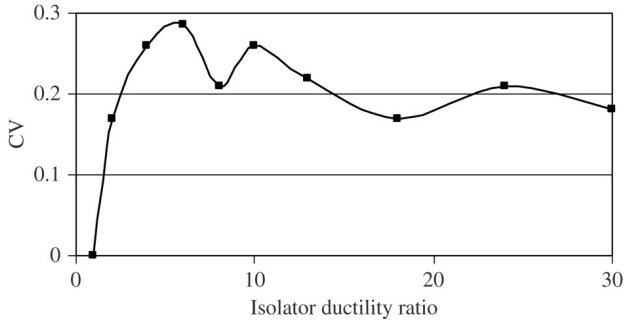

Fig. 1. Coefficient of variation (CV) for all earthquakes and systems.

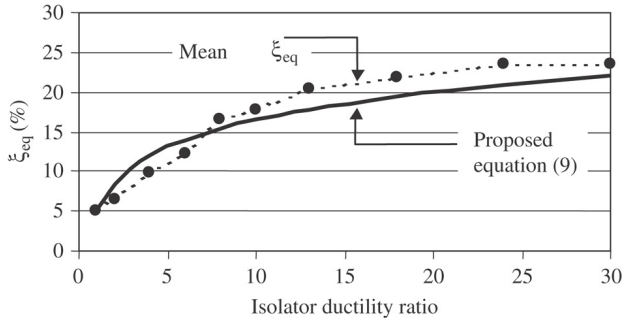

Fig. 2. Mean equivalent damping ratio for all earthquakes and systems.

velocity sensitive spectral region, where the damping effect is more pronounced.

The $\bar{\xi}_{eq}(\mu_b)$ ratio distribution over the whole range of μ_b is shown in Fig. 2. For low values of inelastic displacement demands, $\bar{\xi}_{eq}$ increases very rapidly up to about $\mu_b = 10$. For higher displacement demands, $\bar{\xi}_{eq}$ tends to be asymptotic. Fig. 3 shows a typical curve for the hysteretic energy dissipated by the isolator bearing (E_h), normalized to the input energy (E_i), over the whole range of μ_b. The same trend can be observed from Figs. 2 and 3, and is quite similar for all earthquakes and systems considered in this study. E_h/E_i tends to one only when the bearing dissipates the whole input energy, but this is not the case because of the contribution to the energy dissipation of the piers, abutments and foundation. The influence of μ_b on ξ_{eq} derived from one cycle of steady response to harmonic excitation (proposed in several codes for isolated bridges) is displayed in Fig. 4 for $\alpha = 0.05$ and 0.1, and does not correspond to the curve trend of Eq. (9) or curve trend shown in Fig. 3. Contrary to expectations, the damping ratio decreases when the maximum displacement of the bearing increases for $\mu_b > 6.0$.

Since $\bar{\xi}_{eq}$ increases very rapidly for low μ_b ratios and then is rather uniform, it seems reasonable to fit $\bar{\xi}_{eq}(\mu_b)$ to a logarithmic curve. After data fitting, the following expression is proposed:

$$\xi_{eq} = 0.05 + 0.05\ln(\mu_b). \tag{9}$$

This expression has an adequate minimum value of the equivalent damping ratio, namely $\xi_{eq} = 0.05$ for $\mu_b = 1.0$, since 5% viscous damping is a common value recommended for rubber bearings without a lead core.

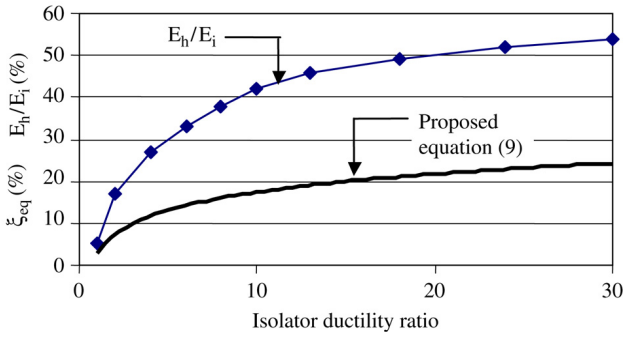

Fig. 3. Hysteretic energy dissipated by the isolator normalized to input energy, and proposed equivalent damping ratio.

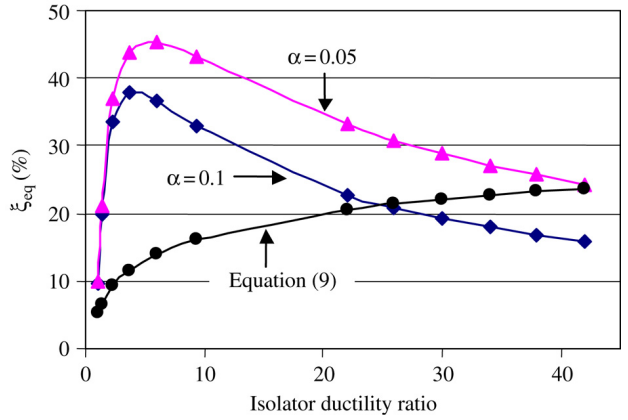

Fig. 4. ξ_{eq} from one cycle of steady-state response to harmonic excitation and the proposed equation.

3.1. Comparison of the equivalent linearization parameters

A comparison of some of the existing models for determining k_{ef} and ξ_{eq} is given in Fig. 5 ($\alpha = 0.1$ is assumed, typical for LRB bearings). The flexibility produced by k_{ef} is represented in terms of the ratio of the effective period to the initial period (T_{ef}/T_1). If $\mu_b < 15$, the secant stiffness model leads to a more flexible system, and the contrary is true for higher ductility ratios. A linear trend represents the Iwan's $(T_{ef}/T_1) - \mu_b$ relationship, giving rise to very flexible systems for $\mu_b > 15$ compared to other models.

For high ductility ratios, ξ_{eq} derived from Kowalsky's expression and from the steady-state harmonic response diminishes with increasing inelastic displacements. In contrast, ξ_{eq} obtained with the equation proposed (9) and with Iwan's model resembles the trend of the hysteretic energy dissipated by isolator bearings.

However, the comparison of the different expressions for computing ξ_{eq} does not provide enough information for reaching conclusions about the adequacy of the prediction of maximum displacement. The response is affected not only by the system energy dissipation capacity but also by the system stiffness k_{ef} and ground acceleration characteristics. A displacement overestimation derived from a reduced value of ξ_{eq} can be mitigated by an overestimation of k_{ef}. In order to compare the adequacy of the existing linear equivalent models,

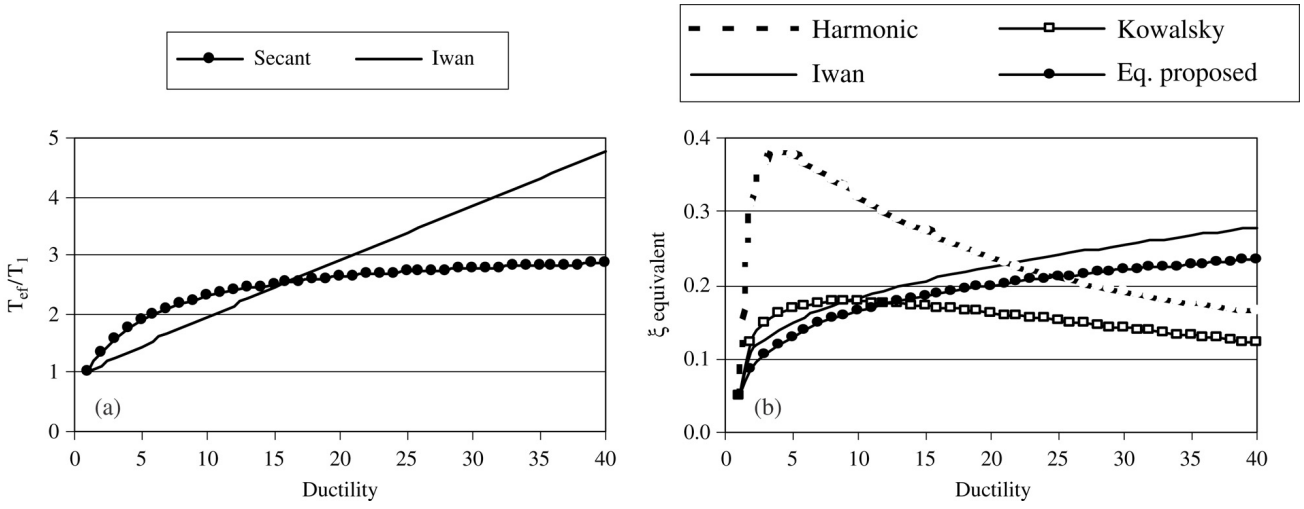

Fig. 5. Comparison of T_{ef} and ξ_{eq} for different equivalent linearization models.

a β factor that includes the combined influence of ξ_{eq} and k_{ef} is proposed.

The amplification factor (β_k) of the elastic displacement spectral ordinates derived from the usage of k_{ef}, for the mid-period range of 0.4–3.0 s and firm soils, is somewhat proportional to,

$$\beta_k \propto (S_d)_{\text{elastic}}\sqrt{k_1/k_{ef}}. \tag{10}$$

The reduction factor (β_ξ) of the elastic displacement spectral ordinates produced by ξ_{eq} can be estimated by substituting the equivalent damping ratio in the following expression [6]:

$$\beta_\xi = \left(\frac{7}{2+\xi_{eq}}\right)^{0.35}. \tag{11}$$

Thus, the combined influence of system stiffness and hysteretic damping can be estimated approximately as:

$$\beta = (S_d)_{\text{elastic}}\sqrt{\frac{k_1}{k_{ef}}}\left[\frac{7}{2+\xi_{eq}}\right]^{0.35}. \tag{12}$$

It is evident that actual spectral displacement demands depend on the characteristics of ground motion and on the numerical evaluation of the hysteretic damping over the total duration of ground acceleration; nevertheless, for assessment purposes, β is a better estimator than ξ_{eq} or k_{ef} by themselves. Fig. 6 shows the comparison of equivalent models in terms of β obtained from period ratio instead of stiffness ratio, i.e.,

$$\beta = \frac{T_{ef}}{T_1}\left(\frac{7}{2+\xi_{eq}}\right)^{0.35}. \tag{13}$$

During ground motion loading, displacements are significantly smaller than $x_{\max}$ most of the time. Because of this, the steady-state harmonic response method, based on the cycle of response at $x_{\max}$, underestimates maximum displacements for low ductility ratios. Chopra and Goel [14] have also reported displacement underestimation, with errors approaching 50%. On the other hand, the equation proposed predicts the largest displacements of all methods for $\mu_b < 15$ (Fig. 6), providing

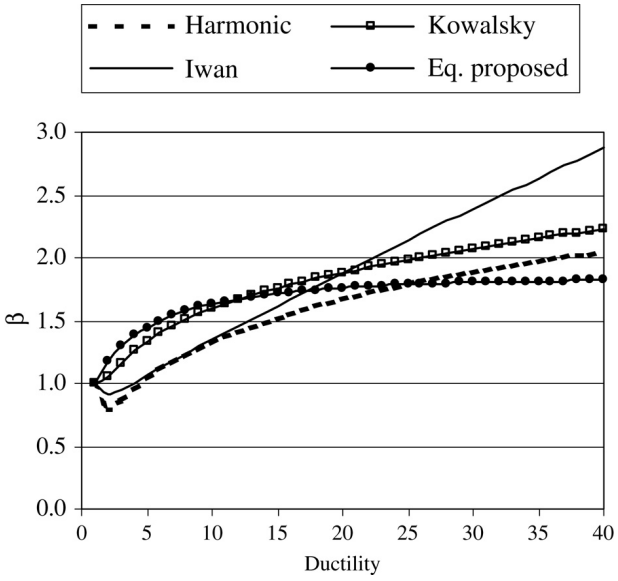

Fig. 6. Comparison of different equivalent linearization models for the combined influence of system flexibility and hysteretic damping.

a better fit to inelastic time-history displacements as presented in Section 5. For high ductility ratios, Iwan's model gives the largest displacements and the proposed equation leads to the smallest displacement. The displacement increment obtained with Kowalsky's and steady-state harmonic response methods for the high ductility range is caused by the anomalous reduction of ξ_{eq} for large displacement demands.

The equivalent damping model proposed presents a clear improvement in respect to some of the linearization techniques available (and presented in the paper) in the particular case of bridges supported in isolating devices with bi-linear hysteretic characteristics. In fact, Eq. (9) is the only one that is derived from the particular characteristics of bridges supported on bi-linear hysteretic bearings, for the complete ductility ratio range that is expected during an earthquake ground motion for this type of device. In contrast to other methods, the trend in the equivalent damping ratio obtained (see Figs. 4–6) seems

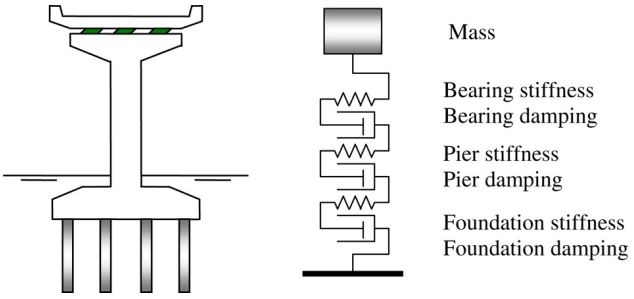

Fig. 7. Idealized single degree of freedom system.

like the trend in hysteretic energy bearing dissipation over the whole range of inelastic displacement demands (Fig. 3). Unlike the models that are based on optimisation of the minimum differences between the inelastic and elastic responses, the empirical expression proposed is rational and simple, and ties the physical behavior of this type of systems. Besides the good trend when compared to bearing dissipation, Eq. (9) also provides a displacement prediction that is in good agreement with inelastic time-history displacements, as can be seen in the examples presented in Section 5. In addition, Eq. (9) can easily be incorporated into the direct displacement-based design framework, as presented in the design example.

3.2. Equivalent damping ratio for the isolator–pier–foundation system

If the bridge superstructure is presumed to be relatively rigid in comparison to the combined stiffness of bearings and piers, the bridge model can be simplified as a SDOF system consisting of the mass of the superstructure and the force recovery and energy dissipation characteristics provided by the isolation devices and piers (Fig. 7).

The algebraic summation of isolator damping ξ_{eq} and pier damping (ξ_p) cannot be assumed, as the isolation bearings are connected to piers in series. Instead, the damping ratio of the isolation–pier system can be determined by the proportional energy damping method, originally proposed in [15],

$$(\xi_{eq})_i = \frac{\sum_j^n (\boldsymbol{\varphi}_i^T)_j \mathbf{C}_j (\boldsymbol{\varphi}_i)_j}{2\boldsymbol{\varphi}_i^T \mathbf{K}_T \boldsymbol{\varphi}_i} \tag{14}$$

where $(\xi_{eq})_i$ is the equivalent damping ratio of mode i, $(\boldsymbol{\varphi}_i)_j$ is the mode shape vector of subsystem j corresponding to mode of vibration i, $\mathbf{C}_j$ is the damping matrix of the subsystem j, $\boldsymbol{\varphi}_i$ is the mode shape vector of the overall system of the mode of vibration i, and $\mathbf{K}_T$ is the stiffness matrix of the overall system. If piers and abutments are presumed to be fixed at their base, and the superstructure is assumed to be rigid, the mode shape vectors for the isolation–pier bearings system are,

$$\boldsymbol{\varphi}_i = \begin{Bmatrix} 1 + \dfrac{(k_{ef})_j}{(k_p)_j} \\ \dfrac{(k_{ef})_j}{(k_p)_j} \end{Bmatrix} x_j \tag{15}$$

$$(\boldsymbol{\varphi}_i)_j = \begin{Bmatrix} 1 \\ \dfrac{(k_{ef})_j}{(k_p)_j} \end{Bmatrix} x_j \tag{16}$$

where x_j is the lateral displacement degree of freedom of subsystem j, k_{ef} is the effective stiffness of the isolator unit j, and k_p is the lateral stiffness of pier or abutment j. If the limit state under consideration allows piers to be damaged, then an effective stiffness of a damaged pier has to be considered according to the maximum ductility allowed. The stiffness matrix of the overall system is,

$$\mathbf{K}_T = \begin{pmatrix} (k_{ef})_j & -(k_{ef})_j \\ -(k_{ef})_j & (k_{ef})_j + (k_p)_j \end{pmatrix}. \tag{17}$$

The damping matrix $\mathbf{C}_j$ is the sum of the proportional damping matrix of the subsystem without isolation bearings $\mathbf{C}_s$ and the non-proportional damping matrix due to the hysteretic damping provided by the isolator bearings $\mathbf{C}_b$,

$$\mathbf{C}_j = \mathbf{C}_s + \mathbf{C}_b. \tag{18}$$

The resultant damping matrix $\mathbf{C}_j$ is non-proportional and the following product is not a diagonal matrix, whose off-diagonal terms, c_{ij}, are not necessarily zero,

$$(\boldsymbol{\varphi}_i^T)_j \mathbf{C}_j (\boldsymbol{\varphi}_i)_j = \begin{pmatrix} c_{11} & c_{12} & c_{13} \\ c_{21} & c_{22} & c_{23} \\ c_{31} & c_{32} & c_{33} \end{pmatrix}. \tag{19}$$

As a consequence, uncoupling of the equations of motion is not possible. According to [9,15], the influence of the off-diagonal terms on the response is small if the hysteretic damping is less than 30%, and can be ignored because its relevance on the results is negligible.

The equation of motion for an SDOF hysteretic system is similar to that of a viscous system with a hysteretic damping coefficient c_h equal to $2\xi_h k$, in which ξ_h represents the hysteretic damping ratio. It has been found [9,15] that the amplitude and phase angle of the transfer function are quite similar for hysteretic and viscous systems, and the difference in the response to a transient excitation is practically identical for both systems, except for the long period region. So that ξ_{eq} and ξ_p can be considered as hysteretic instead of viscous, and the corresponding hysteretic coefficients are $(c_h)_b = 2\xi_{eq} k_{ef}$ and $(c_h)_p = 2\xi_p k_p$.

Thus, $\mathbf{C}_j$ for the isolation–pier system, ignoring the off-diagonal terms is,

$$\mathbf{C}_j = \begin{pmatrix} (2\xi_{eq} k_{ef})_j & 0 \\ 0 & (2\xi_p k_p)_j \end{pmatrix}. \tag{20}$$

If piers are allowed to be damaged, then the equivalent damping ratio of piers has to be used.

The equivalent damping ratio for the isolator–pier system $(\xi_{eq})_s$ obtained by substituting Eqs. (15)–(17) and (20) in (14) is given by,

$$(\xi_{eq})_s = \frac{\xi_{eq} + \xi_p \frac{k_{ef}}{k_p}}{1 + \frac{k_{ef}}{k_p}}. \tag{21}$$

As the isolation units over one pier or abutment undergoes the same lateral displacement, the bearing total stiffness is computed as the sum in parallel of the stiffness of each of the n isolation devices on the pier,

$$k_{ef} = \sum_{k=1}^{n} (k_{ef})_k. \tag{22}$$

The total lateral stiffness of the combined isolation–pier system $(k_{ef})_s$ is the sum in series that is obtained as,

$$(k_{ef})_s = \frac{k_p \sum_{k=1}^{n} (k_{ef})_k}{k_p + \sum_{k=1}^{n} (k_{ef})_k}. \tag{23}$$

If the flexibility and energy dissipation of the foundation are considered, $(\xi_{eq})_s$ of the combined isolation–pier–foundation system derived from Eq. (14) is:

$$(\xi_{eq})_s = \frac{\xi_{eq} + \frac{\xi_p k_{ef}}{k_p} + \frac{\xi_{fh} k_{ef}}{k_{fh}} + \frac{\xi_{f\theta} k_{ef} L^2}{k_{f\theta}}}{1 + \frac{k_{ef}}{k_p} + \frac{k_{ef} L^2}{k_{fh}}} \tag{24}$$

where ξ_{fh} is the equivalent damping ratio corresponding to horizontal vibration of the foundation, $\xi_{f\theta}$ is the equivalent damping ratio corresponding to rotational vibration of the foundation, k_{fh} is the horizontal foundation stiffness, $k_{f\theta}$ is the rotational foundation stiffness, and L is the column height.

$(k_{ef})_s$ of the combined isolation–pier-foundation system is obtained by summing in series the stiffness provided by the foundation, pier and isolation bearing,

$$(k_{ef})_s = \frac{1}{\frac{1}{\left(\sum_{k=1}^{n} k_{ef}\right)_k} + \frac{1}{k_p} + \frac{L^2}{k_{f\theta}}}. \tag{25}$$

4. Procedure for bridges on hysteretic isolators

The proposed methodology is intended for regular bridges supported on bi-linear hysteretic isolation bearings. The superstructure is presumed to be relatively rigid in comparison with the stiffness of piers and abutments, and it is assumed that dynamic response of the bridge can be predicted quite accurately with an SDOF system. A sketch of the idealized model is shown in Fig. 7.

Due to good correlation between strain and damage, the design methodology is based on strain control. The allowable strains should be associated with specific values of structural response that can be accurately predicted and physically measured in an actual structure. According to displacement-based design, the structural response associated with strain control is defined by the structure's lateral displacements. If concrete and steel reinforcement strains are considered as damage indicators of bridge concrete piers, the limit states can be related to lateral pier top displacements. In the case of isolated bridges, limitations to bearing shear displacement must also be considered. Thus, the structural performance is controlled by specifying a target bearing shear displacement (x_b) and a target pier top displacement (x_p). The maximum total displacement of the system is $x_t = x_p + x_b + x_f$, where the last term is the contribution of the foundation's flexibility. In contrast to force-based design, the end result of the displacement-based design procedure is the required stiffness, which is determined from the elastic spectrum by means of x_t and $(\xi_{eq})_s$.

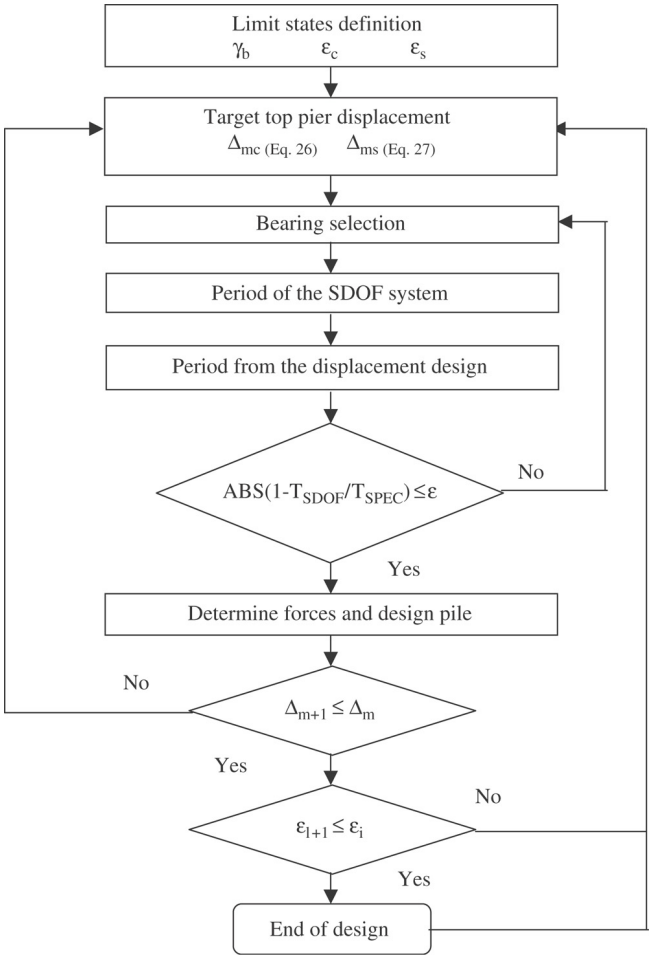

Fig. 8. Flowchart for the displacement-based design for isolated bridges.

The procedure flowchart is presented in Fig. 8 and the step by step procedure description follows.

1. *Limit states.* Define the number of limit states that should be checked, and the isolator shear strain (γ_b), concrete compression strain (ε_c), and steel reinforcement strain (ε_s) corresponding to each limit state.

2. *Target pier top displacement.* After defining preliminary sections of piers, the maximum displacement can be obtained by means of the following strain–displacement relationships developed by Priestley for reinforced concrete piers [4]. The target displacement (Δ_m) is the lesser of Eqs. (26) and (27),

$$\Delta_m = \left(\frac{\varepsilon_c}{c} - \phi_y\right) L_p (L - 0.5 L_p) + \frac{\phi_y L^2}{3} \tag{26}$$

$$\Delta_m = \left(\frac{\varepsilon_s}{D' - c} - \phi_y\right) L_p (L - 0.5 L_p) + \frac{\phi_y L^2}{3} \tag{27}$$

where c is the neutral axis depth, which may be arbitrarily assumed or estimated from Eq. (28) for circular columns and (29) for rectangular columns,

$$c = D\left(\frac{0.65P}{f_c' A_p} + 0.24\right) \tag{28}$$

$$c = h\left(\frac{0.85P}{f_c' A_p} + 0.25\right). \tag{29}$$

L_p is the plastic hinge length given by [4]:

$$L_p = 0.08L + 0.022\, f_y d_{bl} \geq 0.044\, f_y d_{bl} \tag{30}$$

ϕ_y is the yield curvature $= \phi_y = \frac{\varepsilon_y}{c} \simeq \frac{2.45\varepsilon_y}{D}$, L is the column length, D' is the distance from the extreme tension steel fiber to the extreme concrete compression fiber, ε_y is the longitudinal reinforcement yield strain, and d_{bl} is the diameter of longitudinal reinforcement.

3. *Bearing selection*. The minimum in-plan area of the bearing (A_r) is determined by service load conditions, and the lead core area A_l should be $0.02A_r \leq A_l \leq 0.1A_r$. Then assume the height (h) of the bearing and the diameter of the lead core. It is important to comply with the geometric and design recommendations for LRB bearings proposed by codes.

The force that LRB bearings are able to transmit (F_b) can be computed as the sum of the force transmitted by the rubber (F_r) and the force transmitted by the lead core F_l,

$$\text{before yielding:} \quad F_b = F_r + F_l = A_r G_r \gamma + A_l \tau \tag{31}$$

$$\text{after yielding:} \quad F_b = A_r G_r \gamma + A_l \tau_y + A_l \frac{G_2}{G_1}(\tau - \tau_y) \tag{32}$$

where G_1 and G_2 are the elastic and plastic shear stiffness of lead core alone, respectively.

The target bearing displacement x_b is given directly by the product of the total neoprene height $h_r = \sum_i t_i$ and the maximum shear strain γ_b, ($x_b = h_r \gamma_b$).

4. *Period of the SDOF system.* The isolated bridge period $(T_{ib})_{\text{SDOF}}$ is obtained from the well-known expression for SDOF systems, using the total lateral stiffness of the isolated bridge $(k_{ef})_s$ (Eq. (23) or (25)). $\mathbf{K}_p$ is estimated from the basic mechanical principles and k_{ef} is obtained from Eq. (33):

$$k_{ef} = \frac{F_o}{x_{\max}} + k_2 \tag{33}$$

where the post-yielding stiffness (k_2) and the characteristic dissipator strength (F_o) are,

$$k_2 = k_r\left(1 + 10\frac{A_l}{A_r}\right) = G_r A_r \gamma\,(1 + 10\lambda) \tag{34}$$

$$F_o = A_l \tau_y (1 - \alpha). \tag{35}$$

After substituting in (33), the effective stiffness of the isolators is,

$$k_{ef} = \frac{A_l \tau_y (1 - \alpha) + A_r G_r \gamma_b (1 + 10\lambda)}{x_b} \tag{36}$$

and the foundation's flexibility (k_f) is,

$$k_f = F_b / x_f = \frac{F_b}{L \tan(F_b L / k_{f\theta}).} \tag{37}$$

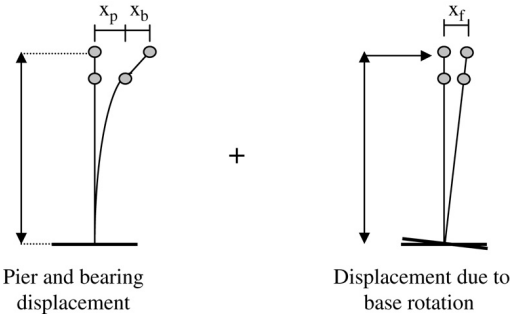

Fig. 9. Total displacement of the system.

Refer to Fig. 9 for the meaning of the parameters. For small rotations,

$$k_f = \frac{F_b}{L(F_b L / k_{f\theta})} = \frac{k_{f\theta}}{L^2}. \tag{38}$$

5. *Period from the displacement design spectra*. The isolated bridge period is then determined from the design spectra $(T_{ib})_{\text{SPEC}}$ by selecting the appropriate damping curve $(\xi_{eq})_s$ and the total system displacement (x_t).

6. *Adjust bearing characteristics*. Periods obtained in steps 4 and 5 must be equal. If they are not, then the isolator properties should be modified. The new bearing area may be obtained by equating the force transmitted by the bearing to the force derived from the spectrum,

$$A_r G_r \gamma_b + A_l \tau_y + A_l \frac{G_2}{G_1}(\tau - \tau_y) = (k_{ef})_s x_t \tag{39}$$

in which $(k_{ef})_s$ is given by,

$$(k_{ef})_s = \left(\frac{2\pi}{(T_{ib})_{\text{SPEC}}}\right)^2 \frac{W}{g}. \tag{40}$$

If $\lambda = A_l / A_r$, the new bearing area is obtained with,

$$A_r = \frac{(k_{ef})_s x_t}{G_r \gamma_b + \lambda\left[\frac{G_2}{G_1}(\tau - \tau_y) + \tau_y\right]}. \tag{41}$$

Steps 4–6 would be repeated until the convergence criteria is satisfied ($\varepsilon = 0.03$, for instance),

$$\left|1 - \frac{(T_{ib})_{\text{SDOF}}}{(T_{ib})_{\text{SPEC}}}\right| \leq \varepsilon. \tag{42}$$

If this criteria is not satisfied by changing the bearing properties, the pier section must be modified.

7. *Determine forces and pier section design.* Since the periods are equal, design forces can then be determined,

$$V_{\text{base}} = k_p x_p \qquad M_{\text{base}} = V_{\text{base}} L. \tag{43}$$

Determine the longitudinal and transverse reinforcement. If the pier section is not appropriate for resisting the design forces, repeat steps 2–7 until the section pier is appropriate.

8. *Lateral displacements verification*. Determine the updated pier top displacement $(\Delta_m)_u$ with the latest c, ε_s and ε_c values. If $\Delta_m \geq (\Delta_m)_u$, then repeat steps 2–7 with $(\Delta_m)_u$ as the initial displacement.

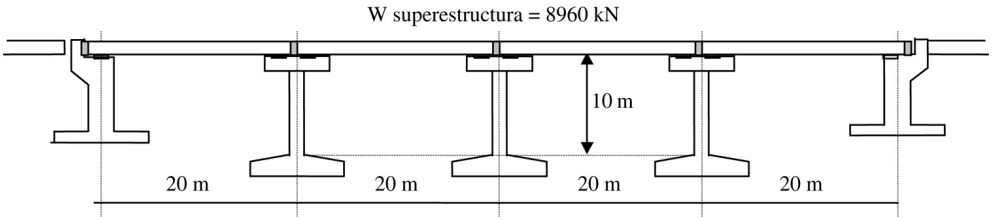

Fig. 10. Four simply supported span bridge model.

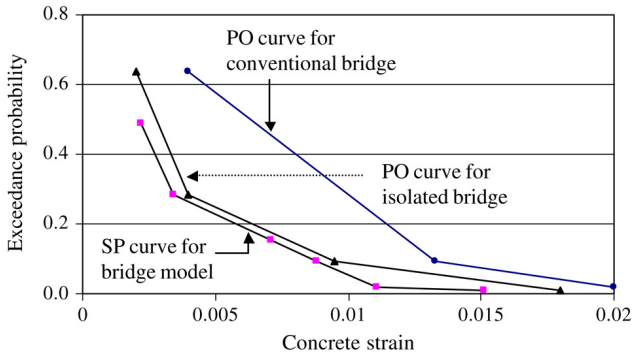

Fig. 11. Performance space for conventional and isolated bridges.

9. *Materials strain verification.* Check if concrete and steel strains fulfill the limit states requirements. Curvature ductility μ_θ must be calculated first (Eq. (44)), then maximum curvature ϕ_m, with Eq. (45), and concrete and steel strains by means of Eq. (46) [4]:

$$\mu_\theta = 1 + \frac{\mu_\Delta - 1}{3L_p} L \tag{44}$$

$$\phi_m = \mu_\theta \phi_y \tag{45}$$

$$\varepsilon_c = \phi_m c \qquad \varepsilon_s = \phi_m \left(D' - c\right). \tag{46}$$

After verifying that ε_s and ε_c fulfil the limit state defined at the beginning, repeat steps 2–9 for other limit states.

5. Examples

First, an example is presented to show the design methodology explained in chapter 4. A four span bridge model supported on LRB bearings, with 10 m heigh piers and rigid abutments, has been considered. The bridge is composed of simply supported spans; the span length is 20 m and the circular concrete piers are assumed to be 1.7 m in diameter, fixed at their bases (Fig. 10). The concrete cylinder's compressive strength is 25 MPa and the yield stress of steel is 400 MPa. The Eurocode 8 displacement design spectra [6] for firm soil is considered. The shear modulus of rubber is 1.0 MPa and the shear yield stress of the lead plug is 10 MPa.

The period of the simple oscillator computed in the first iteration $(T_{ib})_{\mathrm{SDOF}} = 2.11$ s is greater than the period obtained from the design spectrum $(T_{ib})_{\mathrm{SPEC}} = 1.80$ s, and the convergence criteria (Eq. (42)) is not satisfied. Therefore, $(k_{ef})_s$ must be increased by modifying the isolator dimensions (Eq. (41)). After increasing A_r and A_l, $(T_{ib})_{\mathrm{SDOF}} = 1.79$ s, and convergence is reached. Then, the pier section is designed and the longitudinal and transverse reinforcement are determined. Since $(\Delta_m)_u = 0.153$ m, computed with the latest parameters, is less than $\Delta_m = 0.17$ m, a second iteration has to be carried out with $\Delta_m = 0.153$ m as the initial displacement. After a second iteration, $(\Delta_m)_u = 0.146$ m is obtained and accepted. Final results are shown in Table 3.

Since the definition of limit states has social and economic consequences, code committees should propose the number of limit states and their corresponding allowable parameters. In the example, six limit states are proposed arbitrarily to illustrate the consequences of adopting different limit states. The final results are reported in Table 4. The definitive design consists of eight 350 × 350 mm LRB bearings, with a lead core of 89 mm in diameter. The column section is 1.7 m, and the required longitudinal steel ratio is $\rho = 2.6\%$.

According to the conceptual framework for performance-based design, the couples of expected damage levels and expected earthquake intensity are called "Performance Objectives" (PO) and can be represented in the "Performance Space" [16] displayed in Fig. 11. PO curves for conventional and isolated bridges are depicted with discrete points (reported in Ref. [17]) interconnected by straight lines. The "Structural Performance" (SP) curve for the bridge model is displayed in the same figure, where it can be observed that the definitive bridge design satisfies the design requirements represented by the PO curve for non-isolated bridges. In this particular case, the second limit state governs the design; obviously, this conclusion depends on the value assigned to each limit state. If ε_s or γ_b, instead of ε_c, is selected as damage indicators, similar trends for PO curves would be obtained.

The results obtained through the proposed methodology are compared to the "exact" results computed with inelastic time-history analysis, using acceleration time histories compatible with the Eurocode design spectra for firm soil, for 46 systems [12]. The results for maximum displacement of the pier top show that almost all values are located in the ±20% zone. The mean value $\hat{x} =$ is 0.944, that is, the pier displacement is slightly underestimated by the lineal equivalent procedure. The standard deviation $s = 0.110$ and the coefficient of variation, CV = 0.117, reflects the low scatter of the displacements ratio. The base shear is overestimated ($\hat{x} = 1.24$) with the equivalent linearization method. The standard deviation $s = 0.212$ and coefficient of variation CV = 0.151 reflect the major scatter of the shear base ratio.

In [12], the method has also been applied to 5 continuous concrete bridges, with symmetric and asymmetric transverse distributions of stiffness and different pier heights. The dynamic characteristics of the bridges are as follows:

Table 3
Final results

Δ_m (26)	Δ_m (27)	(T_{ib}SDOF)	Δ_m (27)	ε_c (46)	ε_s (46)	ρ (%)
0.153 m	0.143 m	1.79 s	0.146 m	0.0034	0.0072	2.60

Table 4
Limit states proposed, and corresponding final results

Limit state	P_{50} (%)	ρ_{long} (%)	ε_c	ε_s	γ_b	X_b (m)	X_b/X_p
1	50	1.5	0.0022	0.0062	0.8	0.16	1.28
2	28	2.6	0.0034	0.0072	1.0	0.20	1.37
3	15	2.0	0.0071	0.0161	1.5	0.30	1.61
4	10	1.9	0.0088	0.0192	2.0	0.40	1.67
5	2	1.2	0.0111	0.0322	3.0	0.60	2.16
6	1	1.4	0.0151	0.0395	3.5	0.70	1.76
Limit state	ξ_b (%)	ξp (%)	ξ_{ib} (%)	T_{ib} (s)	T_{ib}/T_o	μ_p	μ_b
1	13.9	5.0	10.7	1.97	2.21	1.00	5.9
2	15.0	8.7	12.8	1.79	1.97	1.32	7.4
3	17.0	10.2	14.6	2.25	2.53	1.51	11.1
4	18.5	15.4	17.4	2.35	2.64	2.55	14.8
5	20.5	16.5	19.1	3.00	3.37	2.95	22.2
6	21.3	18.9	20.4	3.00	3.37	4.23	25.9

1. The maximum eccentricity between the center of gravity of the transverse stiffness in the supports and the center of mass of the bridge is less than 12% of the total bridge length.

2. The stiffness of any subsystem pier+isolator is less than twice the stiffness of the contiguous pier+isolator.

3. The difference in mass between two contiguous supports is less than 25%.

4. The bridge skewness is less than 20° in all cases.

5. The percentage of the mass in the first vibration mode is more than 90%.

Comparison with the results from a non-linear analysis shows that the ratio of linear to non-linear displacements in the isolation devices has a mean value between 1.01 and 1.12 (always on the safe side) with a coefficient of variation that is very low (less than 0.14). In the case of the displacement on the top of the piers, the mean value of the ratio of linear to non-linear displacement is in the range 1.07–1.39, with a coefficient of variation equal to 0.34. The greatest differences appear in the estimation of the shear force in the base. In fact, in this case, the mean value is in the range 1.07–1.41, and with a higher coefficient of variation than in the case of displacements. The most important differences occur in the bridges with periods close to the maxima of the response spectra. As seen, however, in all cases (displacements and shear forces) the results from the proposed model remain on the safe side.

In spite of the good agreement obtained in the examples presented, more research is needed to determine the equivalent damping coefficient and the effective stiffness that should be used for earthquake motion of different characteristics; in particular, energy dissipation for concrete elements and other type of hysteretic or viscous devices should be investigated. The limitations imposed on the continuous symmetric and asymmetric bridges should also be kept in mind. Several authors [8,9] have assessed the accuracy of other existing equivalent linearization methods, and small mean errors have been obtained, but dispersion of the results in some cases is substantial, particularly for large levels of inelastic behavior. It can be affirmed that the proposed methodology improves the prediction capability of the linear equivalent model when it is applied to bridges supported on LRB isolators.

6. Conclusions

This paper presents a displacement-based design procedure for bridges supported on isolation bearings with bi-linear characteristics. The proposed method emphasizes strain control by means of the shear displacement of the isolation bearing, and the lateral pier top displacement. The response is estimated directly from the elastic displacement response spectra by use of an effective period and equivalent viscous damping, and is applicable to regular and quasi-regular bridges with rigid superstructures whose response can be idealized as an SDOF.

An equivalent damping ratio, derived from the particular characteristics of bridges supported on bi-linear hysteretic bearings, is proposed. In contrast to other methods, the trend of the equivalent damping ratio obtained seems like the trend of the hysteretic energy bearing dissipation over the whole range of inelastic displacement demands that is expected for this type of device. Unlike the models that are based on optimisation of the minimum differences between the inelastic and elastic responses, the empirical expression (Eq. (9)) proposed is rational and simple, and ties the physical behavior of this type of systems. This equation provides a displacement prediction that is in good agreement with inelastic time-history displacements and can easily be incorporated into the direct displacement-based design framework.

The proposed methodology improves the displacement prediction capability of the linear equivalent model when it

is applied to bridges supported on LRB isolators. The results obtained through the proposed methodology are compared with the "exact" results computed with inelastic time-history analysis, and it has been found that pier displacements are slightly underestimated but base shears are overestimated. Low data scatter is obtained over the whole range of ductility displacement ratio expected for this type of isolator, especially for displacements. In spite of the good agreement obtained in these cases, more research is needed to determine the equivalent linearization parameters for concrete elements and other types of hysteretic or viscous devices, and the influence of earthquake motions of different characteristics.

Acknowledgements

The financial support of Secretary of Public Education from Mexico, PROMEP, Ministry of Science and Technology from Spain, through research projects MAT2002-00849 and MAT2003-05530, are gratefully acknowledged

References

[1] Jara M, Casas JR. Vibration control of bridges. A state of the art and state of the practice. Monografía CIMNE IS-48. Barcelona (Spain): International Center of Numerical Methods in Engineering; 2002 [in Spanish].
[2] Bertero RD, Bertero VV. Performance based seismic engineering: the need for a reliable conceptual comprehensive approach. Earthquake Engineering and Structural Dynamics 2002;31:627–52.
[3] Priestley MJN. Performance based seismic design. In: Proceedings of 12th world conference on earthquake engineering. 2000.
[4] Kowalsky MJ. A displacement based approach for the seismic design of continuous concrete bridges. Earthquake Engineering and Structural Dynamics 2002;31:719–47.
[5] AASHTO. Guide specifications for seismic isolation design. Washington (D.C): American Association of State Highway and Transportation Officials; 1999.
[6] Eurocode 8. Design provisions for earthquake resistance of structures, Part 2: Bridges. ENV 1998-2. Brussels; 1994.
[7] Japan Road Association, 2. 1996 Seismic Design Specifications of Highway Bridges. 1996.
[8] Miranda E, Ruiz-García J. Evaluation of approximate methods to estimate maximum inelastic displacement demands. Earthquake Engineering and Structural Dynamics 2002;31:539–60.
[9] Franchin P, Monti G, Pinto PE. On the accuracy of simplified methods for the analysis of isolated bridges. Earthquake Engineering and Structural Dynamics 2001;30:363–82.
[10] Clough RW, Penzien J. Dynamics of structures. New York: McGraw-Hill International Book Company; 1993.
[11] Iwan WD. Estimating inelastic response spectra from elastic spectra. Earthquake Engineering and Structural Dynamics 1980;8:375–88.
[12] Jara M. Displacement-based seismic design of bridges on isolation devices. Ph.D. thesis. Barcelona: Technical University of Catalunya; 2004 [in Spanish].
[13] Iwan WD, Gates NC. The effective period and damping of a class of hysteretic structures. Earthquake Engineering and Structural Dynamics 1979;7:199–211.
[14] Chopra AK, Goel RK. Evaluation of NSP to estimate seismic deformation: SDF systems. Journal of Structural Engineering 2000; 126(4):482–90.
[15] Roesset JM, Whitman RV, Dobry R. Modal analysis for structures with foundation interaction. Journal of the Structural Division, ASCE 1973; 99(ST3):399–416.
[16] Collins KR, Stojadinovic B. Limit states for performance based design. In: Proceedings of 12th world conference on earthquake engineering. 2000.
[17] Jara M, Casas JR. Methodology for the selection of hysteretic isolation devices for concrete bridges. In: Proceedings of the FIB-symposium, concrete structures in seismic regions. 2003.